Can endohedral transition metals enhance hydrogen storage in carbon nanotubes?

Can endohedral transition metals enhance hydrogen storage in carbon nanotubes?

U. Khalilov[†,§,‖,#,*], U. Uljayev[‖], K. Mehmonov[‖], P. Nematollahi[#], M. Yusupov[‡,⸸,‖,#] and E.C. Neyts[#]

[†] New Uzbekistan University, Tashkent, 100007, Uzbekistan

[§] National Research University TIIAME, Tashkent, 100000, Uzbekistan

[‖] Arifov Institute of Ion-Plasma and Laser Technologies, Academy of Sciences of Uzbekistan, Tashkent, 100125, Uzbekistan

[#] University of Antwerp, Antwerp, 2610, Belgium

[‡] Central Asian University, Tashkent, 111221, Uzbekistan

[⸸] Tashkent International University of Education, Tashkent 100207, Uzbekistan

* e-mail: umedjon.khalilov@uantwerpen.be (Umedjon Khalilov)

Abstract

The safe and efficient use of hydrogen energy, which is in high demand worldwide today, requires efficient hydrogen storage. Despite significant advances in hydrogen storage using carbon-based nanomaterials, including carbon nanotubes (CNTs), efforts to substantially increase the storage capacity remain less effective. In this work, we demonstrate the effect of endohedral transition metal atoms on the hydrogen storage capacity of CNTs using reactive molecular dynamics simulations. We find that an increase in the volume fraction of endohedral nickel atoms leads to an increase in the concentration of physisorbed hydrogen molecules around single-walled CNTs (SWNTs) by approximately 1.6 times compared to pure SWNTs. The obtained results provide insight into the underlying mechanisms of how endohedral transition metal atoms enhance the hydrogen storage ability of SWNTs under nearly ambient conditions.

keywords

hydrogen energy, hydrogen storage, carbon nanotube, endohedral metal atoms, reactive molecular dynamics, hydrogen adsorption.

Introduction

Hydrogen energy is currently regarded as a highly promising renewable energy source due to its environmental friendliness and high efficiency [1-3]. One of the most important challenges in hydrogen energetics is the safe and efficient storage of hydrogen atoms/molecules [3-11]. Various traditional methods of hydrogen storage [12], including compression [13], liquefaction [11,14], physisorption [15,16], hydrides [9,10,17,18] and other methods [2,7,8,15,19,20], are currently being investigated. Nevertheless, the issue of the effective use of hydrogen on a large scale remains a crucial problem that needs to be addressed [1,5,21]. In particular, the storage of compressed and liquified hydrogen is inappropriate for large-scale use due to its low density and high cost at high pressures as well as boiling-off issues at room temperature [3,5,12,21]. In this respect, metal hydrides have the ability to store hydrogen with a high volumetric density [10,17]. However, their gravimetric density is limited due to the presence of heavy transition metals [21]. Moreover, the process of hydrogen absorption, desorption, and release in metal hydrides requires high temperatures and significant energy input [21]. In contrast, complex hydrides possess remarkably high volumetric and gravimetric densities [9,18]. Still, their melting points are in close proximity to cryogenic temperatures (around 200 K), causing them to exist in a liquid phase at room temperature [21].

In recent decades, the physisorption of hydrogen on and in porous materials has been developed to solve the above problems [7,15,16,22,23]. Most of the research related to this method uses metal-organic frameworks (MOFs) [6,19,22,24,25] and various carbon-based nanostructures [8,20,23,26-28] as porous materials. These materials are currently being studied to improve their hydrogen storage capacity by increasing the absorption and adsorption rates of hydrogen atoms or molecules [29]. Carbon-based nanomaterials are especially interesting candidates for hydrogen storage due to their low weight and chemical stability [30-32]. In particular, carbon nanotubes (CNTs) [33] have been proposed as efficient hydrogen storage materials due to their unique properties, such as low density and large surface area [7,28,34-36]. Consequently, significant research has been conducted on hydrogen storage using single- [7,26,37-40] and multiwalled CNTs [30,31,40-42]. Various studies have shown that physisorbed and chemisorbed hydrogen species can be stored in CNTs at gravimetric densities of 0.1–6.3 wt.% and pressures of 0.01–20 MPa [26,27,34,39,40,43-48]. Although CNTs appear to be more efficient at storing hydrogen than metal hydrides, the storage pressure in CNTs is approximately 5 to 10 times higher, resulting in increased storage costs.

Alternatively, various transition metal nanocatalysts adsorbed on the CNT surface are also considered for hydrogen storage [36,42,47,49]. Using this method, the effective storage of hydrogen atoms on the CNT surface due to the chemical dissociation of hydrogen molecules by adsorbed nanocatalysts is being intensively studied [36,42]. In particular, transition metal-doped CNTs can

store hydrogen at gravimetric densities in the range of 3.0 - 7.0 wt.% at a pressure of approximately 0.1 MPa [36]. Despite the high storage capacity achieved even at low hydrogen pressures, the disadvantage of the method is the chemical instability of transition metal-doped CNTs [36]. For instance, an increase in the concentration of Ni nanoparticles on the surfaces of single-walled CNTs (SWNTs) (from 0 to 8 wt.% Ni) leads to an increase in the concentration of chemisorbed H atoms (from 1.61 to 5.25 wt.%), a further increase in the concentration of nickel (12 wt.% Ni) sharply reduces the hydrogen storage capacity of SWNTs (2.99 wt.%), which was explained by the blocking effect due to the association of Ni nanoparticles on the surfaces of SWNTs [47]. On the other hand, this phenomenon can also be associated with a change in the physical properties of the SWNT surface caused by the nanocluster binding nature due to the confinement effect [50]. Because of this effect, endohedral metal atoms bind weakly to the interior of the SWNT wall compared to those adsorbed on the outside of the SWNT, regardless of their catalytic activity [50,51]. Thus, transition metal atoms can form nanoclusters [52-54] or nanowires [55,56] inside a CNT instead of being located separately in the interior [57]. This has resulted in the thorough investigation of the chemical vapor deposition (CVD) growth of these nanoclusters and nanowires inside SWNTs [58], as well as their resulting electronic and magnetic properties [55,56]. Nevertheless, to the best of our knowledge, studies on hydrogen storage on the surface of SWNTs using endohedral transition metals have not yet been conducted.

In this study, we explore for the first time the role of an endohedral transition metal (namely, nickel) in enhancing the hydrogen storage capacity of SWNTs under ambient conditions, i.e., room temperature and atmospheric pressure, by reactive molecular dynamics (MD) simulations.

Computational details

The process of hydrogen storage on SWNTs with endohedral Ni atoms is investigated by employing reactive MD simulations using the LAMMPS package [59]. To describe interatomic interactions in the system, the ReaxFF potential with a previously validated parameter set developed by Mueller is used [60]. In the simulations, a pristine (5,5) nanotube and a (5,5) nanotube with endohedral Ni atoms at different concentrations (i.e., Ni_n@SWNT, where $n=0, 1, 5, 13$) are selected as model SWNTs (Fig. 1). The diameter of the SWNTs is 6.93 Å, which is within the range of experimentally obtained nanotube diameters (6.3–7.9 Å) [61]. Periodic boundary conditions are applied along the z-axis, which represents the length of the SWNT (27.25 Å), allowing the simulation of infinitely long SWNTs.

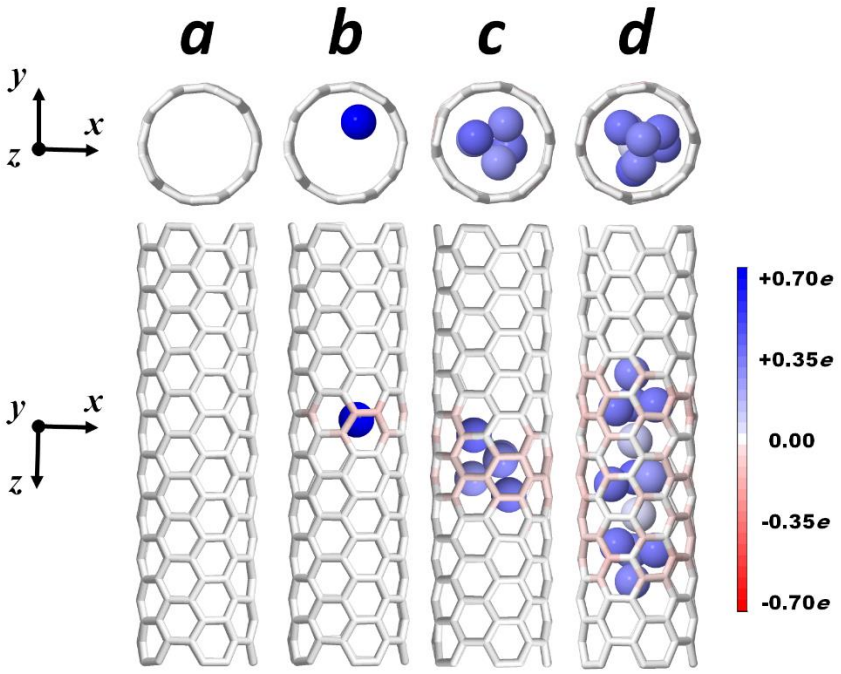

Figure 1. *Top and side views of (a) pristine SWNT, (b) Ni@SWNT, (c) Ni_5@SWNT, and (d) Ni_{13}@SWNT. SWNT and Ni atoms are represented in sticks and balls, respectively. The system atoms exhibit partial charges ranging from -0.7e to +0.7e, depicted by a color spectrum from red to blue, indicating the conversion from electron-rich to electron-poor regions.*

As a result, the filling or volume fraction of endohedral Ni atoms in the SWNT is used (instead of their concentration); hence, this fraction is independent of the length of the SWNT. The volume fraction of endohedral Ni atoms inside SWNT is calculated by dividing the average volume of Ni atoms by the effective volume of SWNT (in %). The average volume of each Ni atom is determined using the van der Waals radius, which is approximately 1.63 Å [62]. The effective volume of SWNT is calculated using the concept of the effective diameter [63], i.e., $d_{eff} = d_{geo} - \sigma_{C-Ni}$, where d_{eff} is the effective diameter of the SWNT, d_{geo} is the geometric diameter of the SWNT (i.e., 6.93 Å), and σ_{C-Ni} is the sigma bond length of C–Ni (i.e., 2.5 Å). According to this formula, the inner volume fraction of the nanotube filled by Ni atom, Ni_5, and Ni_{13} clusters is estimated to be approximately 4, 22, and 56%, respectively. We use these volume fractions instead of the number of Ni atoms inside SWNT to compare our results with experimental data.

Initially, the energy of all model systems is minimized by the conjugated gradient method. Subsequently, the temperature and pressure of the systems are equilibrated to the desired values (300 K and 0 Pa) in the *NpT* ensemble using a Berendsen thermostat and barostat [64] with coupling constants of 100 fs and 5000 fs, respectively. The chosen heating rate (i.e., 1 K/ps) corresponds to a

previously reported range of values (0.1 - 10.0 K/ps) [65,66] and indicates that the deviations in the thermodynamic equilibrium of the model systems are insignificant during the temperature increase. In the case of the physisorption of H_2 molecules on Ni_n@SWNT ($n \in 0, 1, 5$ and 13), the system's temperature is kept at 300 K for 100 ps using a Bussi thermostat [67] with a coupling constant of 100 fs in the canonical *NVT* ensemble.

In the simulations, the pressure of H_2 molecules in the system is calculated as $p = J\sqrt{2\pi MRT}/N_A$, [68] where J is the impingement flux ($nm^{-2}\cdot ns^{-1}$), N_A is Avagadro's number, R is the universal gas constant, M is the molar mass of the H_2 molecule ($kg\cdot mol^{-1}$) and T is the temperature of the system (K). During the *NVT* simulations, H_2 molecules are introduced into the environment surrounding the nanotube surface (~ 5.34 nm^2) at a time interval of 10 ps. The distance between each introduced H_2 molecule and the model system is chosen to be at least 10 Å (i.e., the cutoff radius of the interaction potential). Under these conditions, the impingement flux of the incident H_2 gas (consisting of 300 H_2 molecules) is 18.72 $nm^{-2}\cdot ns^{-1,}$ and its corresponding pressure is approximately 0.174 MPa. The total simulation time for the H_2 physisorption process lasts 3 ns. In all MD simulations, a time step of 0.1 fs is used. The simulations are repeated 5 times for each study case (resulting in a total of 40 simulations), and the final results are obtained by averaging the individual physical quantities.

Results and discussion

SWNT with endohedral Ni atoms. Studying the interaction of endohedral Ni atoms with the inner surface of SWNT is important for a better understanding of the process of hydrogen storage using Ni_n@SWNT. For this purpose, we evaluate the interaction energy of the endohedral Ni atoms with the interior of SWNT, which is defined as $E = E_{Ni_n@SWNT} - (E_{Ni_n} + E_{SWNT})$, where $E_{Ni_n@SWNT}$, E_{Ni_n} and E_{SWNT} are the potential energies of Ni_n@SWNT, Ni_n cluster, and pristine SWNT, respectively [56,69]. Figure 2*a* shows this interaction energy as a function of the volume fraction of Ni atoms inside the SWNT (see red curve). The interaction energies are found to be -43.42±1.93, -30.88±0.96, and -16.40±0.96 $kJ\cdot mol^{-1}$ for volume fractions of 4, 22, and 56%, respectively. This indicates that an increase in the volume fraction of endohedral Ni atoms results in a decrease in their interaction energies with the interior of the SWNT. A similar interaction behavior was obtained for the cases of Fe atom, Fe_2 dimer, and F_{1D} nanowire with the inner wall of an (8,8) CNT, and the calculated DFT energies were found to be -77.19, -11.58, and -2.89 $kJ\cdot mol^{-1}$ per Fe atom, respectively [51]. In general, the interaction behavior between the interior of the SWNT and the metal atoms belonging to the iron family depends on the type of metal. In particular, quantum mechanical calculations showed that the interaction energies of endohedral Co and Fe nanoclusters

with the interior of (5,5) nanotube are 1.22 and 1.44 times higher than the energy of Ni nanocluster at the same concentration [56].

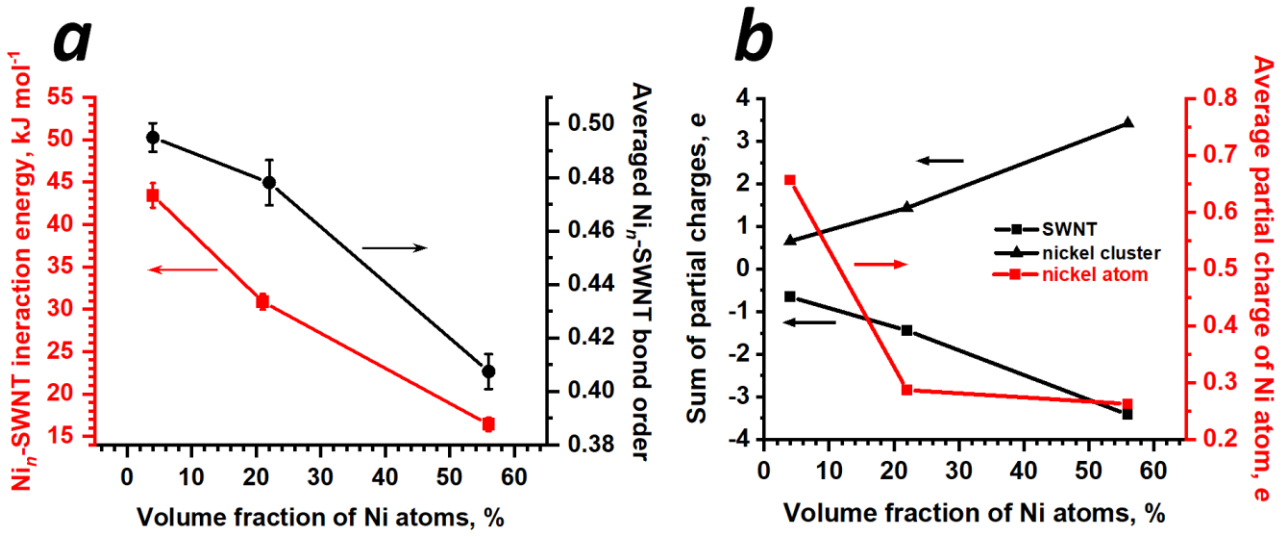

Figure 2. *(a) The absolute values of the negative interaction energy of endohedral Ni atoms with the interior of the SWNT (left, red curve) and the average bond order between Ni and C atoms (right, black curve) as a function of the volume fraction of Ni atoms. (b) The sum of the partial charges of SWNT and Ni atom/cluster (left, black curves) and the average partial charge of Ni atom (right, red curve) as a function of the volume fraction of endohedral Ni atoms.*

The weakening of the interaction can also be seen by a decrease in the average bond order between Ni and C atoms (Fig. 2*a*, black curve). Indeed, the average bond order between Ni···C is 0.495±0.005, 0.478±0.008, and 0.407±0.006 for volume fractions of Ni atoms of 4, 22, and 56%, respectively. It is thus clear that the interaction character between the Ni atoms and the inside wall is noncovalent.

The nature of the interaction between the Ni atom/cluster and the interior of the SWNT can be explained by the confinement effect [50,70] associated with a change in the curvature of the adsorbent surface [71]. In particular, twisting or bending graphene leads to a deformation of the π bonding, which causes the transfer of electrons from the concave side to the convex side, thereby leading to a different distribution of electrons inside and outside the SWNT [51,70,71]. Hence, this phenomenon and the addition of Ni atoms inside the SWNT together influence the partial charges of atoms in the system (see Fig. 2*b* and cf. Fig. 1). In particular, an increase in the volume fraction of Ni atoms leads to an increase in the magnitudes of the sum of the partial charges of the SWNT and Ni cluster, which are found to be between -0.5*e* and -3.5*e* and +0.5*e* and +3.5*e* (see black curves), respectively. However, the average partial charge of individual nickel atoms decreases from 0.67*e* over 0.29*e* to

0.27e for volume fractions of 4, 22, and 56%, respectively (see red curve), which is due to the formation and further strengthening (or an increase in the binding energy) of the Ni-Ni bonds. Indeed, according to quantum mechanical calculations, the binding energies of Ni_2, Ni_{13} and Ni_{55} nanoclusters are found to be between 63.68-215.18, 260.53-411.05 and 338.69-440.97 kJ·mol^{-1}, respectively [71]. Consequently, the electron density between the Ni atoms in the cluster increases, causing a decrease between the Ni and C atoms, eventually leading to a weakening of the interaction between SWNT and endohedral Ni atoms. Therefore, a sharp drop (~2.6 times decrease) in the average partial charge per Ni atom is observed (Fig. 2*b*, red curve) due to the "atom-to-cluster" transition.

In addition, a decrease in the Ni···C interaction energy causes an increase in the mobility of Ni clusters [53,70] and hence most likely does not allow defect formation inside the SWNT by endohedral Ni atoms [53,72]. The simulation results also show that an increase in the volume fraction of Ni atoms leads to an increase in the number of C atoms with nonzero partial charges in the SWNT. In particular, the percentage of these carbon atoms is approximately 66, 86 and 99% for Ni volume fractions of 4, 22, and 56%, respectively. This indicates that a volume fraction of endohedral Ni atoms greater than 56% results in negative nonzero partial charges of almost all carbon atoms in SWNT.

Hydrogen physisorption on SWNT with endohedral Ni atoms. The study of hydrogen storage using SWNTs by physisorption of H_2 molecules is essential for understanding how to easily extract hydrogen to reuse it as an energy source [7,21]. In general, the physisorption of H_2 molecules on pristine SWNT depends strongly on its surface curvature (or diameter) [48,73] and metallicity effects [45,74]. In addition to these effects, our simulation results strongly indicate that the physisorption also depends on the endohedral metal atoms of SWNT. As a specific example, Figure 3*a* illustrates a snapshot of the physisorption process of the H_2 molecules on Ni_5@SWNT (i.e., with a volume fraction of 22%). Here, d_{cut} is the cutoff interaction distance from the surface of SWNT used to estimate the region for stored H_2 molecules (see next paragraph). The figure indicates that the partial charges of Ni and H atoms near SWNT are positive, whereas those of C atoms are negative due to confinement [50,51,57,70] and the endohedral metal effect. Overall, our results show that the sum of the partial charges of SWNT carbon atoms are -2.56e, -3.72e, -5.63e, and -8.60e, nickel atoms are 0.0, 0.85e, 2.35e, and 4.08e, and those of hydrogen atoms are 2.56e, 2.87e, 3.28e, and 4.52e for volume fractions of 0, 4, 22, and 56%, respectively. These changes in the partial charges significantly impact the nonbonded interactions between H_2 molecules and SWNT.

The nonbonded interaction energy of a single H_2 molecule with pristine or Ni containing SWNT (Ni_n@SWNT, $n \in 0, 1, 5$ and 13) is depicted in Figure 3*b*, which is calculated as $E = E_{H_2+Ni_n@SWNT} - (E_{H_2} + E_{Ni_n@SWNT})$, where $E_{H_2+Ni_n@SWNT}$, E_{H_2}, and $E_{Ni_n@SWNT}$ are the potential energies of the

whole system, H_2 molecule and Ni_n@SWNT, respectively [54,69]. The lowest interaction energy (i.e., most negative value) between the Ni_n@SWNT and H_2 molecule is found to be -9.87, -10.01, -10.72 and -12.02 kJ·mol^{-1} at approximately 2.24, 2.44, 2.34, 2.34 Å from the SWNT surface, for volume fractions of 0, 4, 22, and 56%, respectively. Overall, the area of the energy curve increases by increasing the number of endohedral atoms (see Fig. 3*b*).

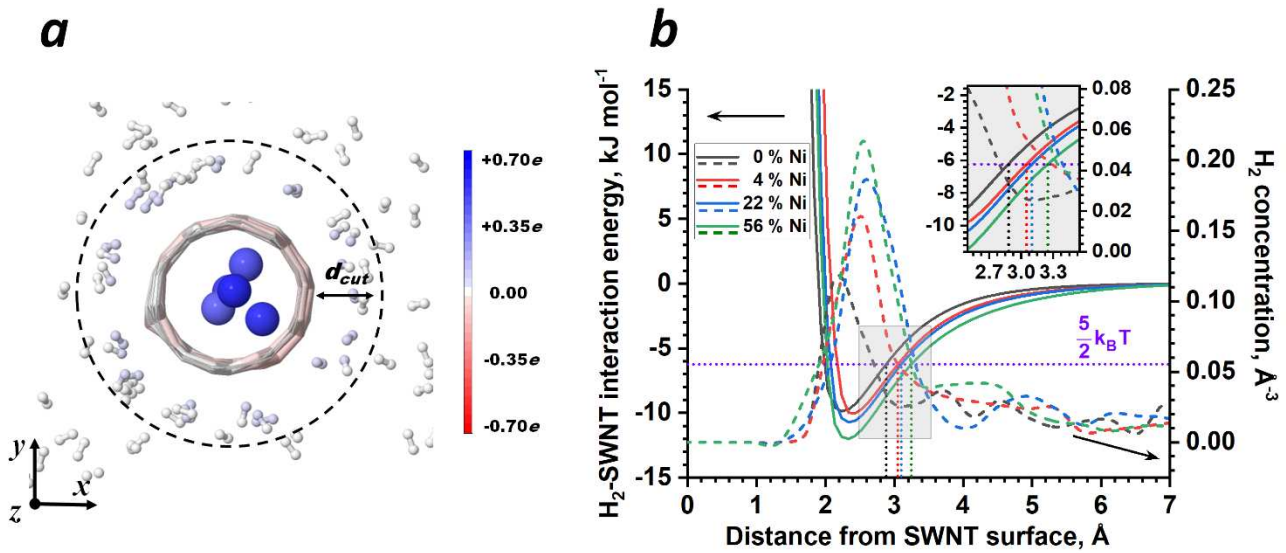

Figure 3. *(a) The cross-section of Ni_5@SWNT (i.e., the volume fraction of 22%) with surrounding H_2 molecules. The system atoms exhibit partial charges ranging from -0.7e to +0.7e, depicted by a color spectrum from red to blue, indicating the transition from electron-rich to electron-poor regions. The cutoff interaction distance (d_{cut}) from the surface of Ni_5@SWNT is 3.1 Å. (b) The distribution of the interaction energy between a single H_2 molecule and Ni_n@SWNT (solid curves) as well as the concentration of H_2 molecules (dashed curves), as a function of d_{cut}. Each interaction energy curve is an average of 6 energy profiles obtained from trajectories equally distributed perpendicular to the nanotube's length (z-axis).*

To determine the cutoff interaction distance from the surface of the SWNT (d_{cut}) for physisorbed H_2 molecules, we use the energy point where the average kinetic energy of the H_2 molecule and its interaction energy with SWNT equals. The average kinetic energy of an H_2 molecule ($\frac{5}{2}k_BT$, where k_B is the Boltzmann constant and T is the room temperature) is found to be approximately 6.23 kJ·mol^{-1} (see dashed line in Fig. 3*b*). This value is very close to the values reported by experiment (~6 kJ·mol^{-1} [75]) and quantum-mechanical calculation results (6.56 kJ·mol^{-1} [46]) for H_2 adsorption energy on

SWNT. The change in n of the Ni_n@SWNT system leads to alterations in the shape of the interaction energy profile (as mentioned above), consequently varying the cutoff interaction distance. In particular, as can be seen in Fig. 3*b* (dotted lines), d_{cut} is found to be approximately 2.88, 3.05, 3.10 and 3.25 Å for $n = 0$, 1, 5 and 13 (or volume fractions of 0, 4, 22 and 56%), respectively. The obtained cutoff distance for the case of pristine SWNT (2.88 Å) is found to be within the experimental and theoretical adsorption distances for H_2 molecules on SWNTs (i.e., 2.7-3.1 Å) [46,75].

For all volume fractions, the distribution of H_2 concentration (represented by the dashed curves in Fig. 3*b*) reveals that while the distribution extends up to 7 Å, all peaks are located within 3.25 Å from the surface of the SWNT, corresponding to the largest d_{cut}. Specifically, these peaks are found at 0.12, 0.16, 0.18, and 0.21 $Å^{-3}$ for volume fractions of 0, 4, 22, and 56%, respectively. The H_2 concentrations, obtained within the specific cutoff distances of each case, contribute to calculating the gravimetric density of physisorbed H_2 molecules.

Figure 4*a* illustrates how the gravimetric density of physisorbed H_2 molecules varies based on the volume fraction of endohedral Ni atoms within the SWNT. The gravimetric density is determined as $m_H N_H \times (m_H N_H + m_C N_C + m_{Ni} N_{Ni})^{-1} \times 100\%$, where m and N are the mass and number of H, C or Ni atoms [76].

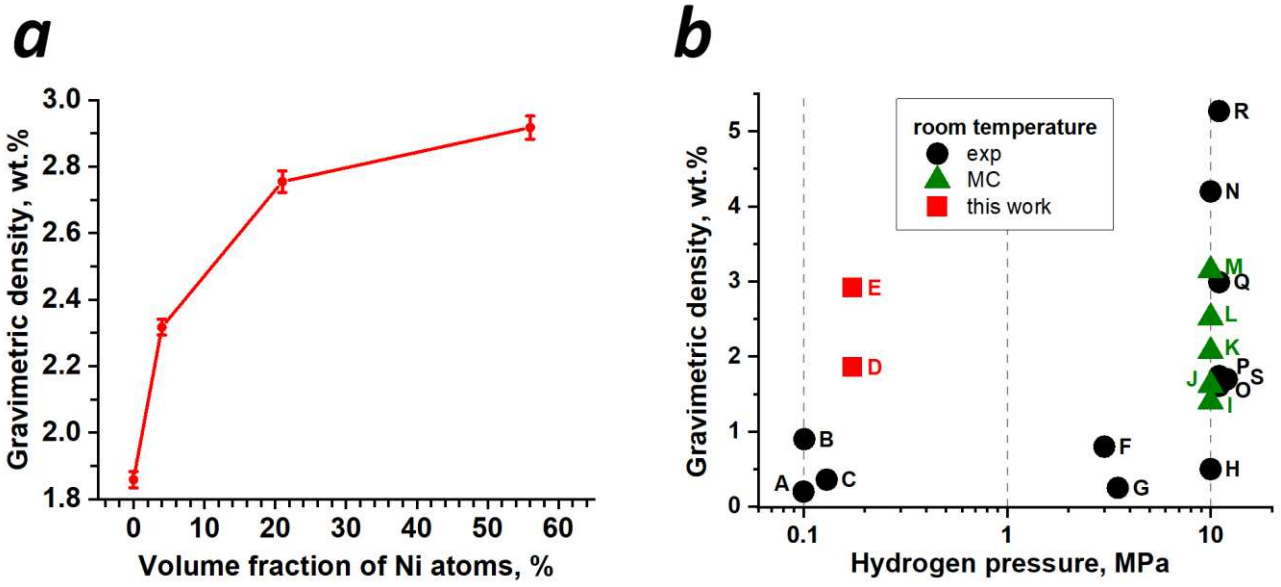

Figure 4. *(a) The average gravimetric density of physisorbed H_2 molecules as a function of the volume fraction of endohedral Ni atoms. (b) Comparative analysis of gravimetric densities for hydrogen adsorption on SWNT obtained from literature data as a function of hydrogen pressure at approximately room temperature.*

As shown in Figure 4*a*, the gravimetric density of the physisorbed H_2 molecules on pristine SWNT is 1.86 wt.%. This value corresponds to a degree of hydrogen coverage (N_H/N_C) equal to 22.72%, which is in good agreement with experimental (21-25% [26]) and simulation (22% [69]) data for pristine SWNTs at room temperature. In the case of SWNTs with endohedral Ni atoms at volume fractions of 4, 22, and 56%, the gravimetric density (or degree of hydrogen coverage) increases to 2.32 wt.% (29.09%), 2.75 wt.% (37.73%) and 2.92 wt.% (46.36%), respectively, i.e., by factors of 1.25 (1.28), 1.48 (1.66) and 1.57 (2.04) higher than that of pristine SWNT. The obtained results strongly indicate that an increase in the number of endohedral Ni atoms leads to an increase in the degree of surface coverage of SWNT with physisorbed H_2 molecules.

Please note that experimental studies typically focus on the average gravimetric density of SWNT forests, whereas our simulation work considers the gravimetric density of individual SWNTs, without accounting for environmental effects. To make a qualitative comparison, we review relevant literature data (detailed in Table S1) regarding gravimetric densities obtained in our simulations. Specifically, we select the values for pristine SWNT (1.86 wt.%) and SWNT with the highest concentration of endohedral Ni atoms (2.92 wt.%), denoted by D and E in Figure 4*b*, respectively. According to experimental and theoretical/computational reports [26,27,34,39,40,43-47], gravimetric densities of hydrogen on SWNTs are observed in the range of 0.2-5.27 wt.% at hydrogen pressures of 0.1-12 MPa and about room temperature (see Fig. 4*b* and Table S1). As is clear from the figure, most of the obtained higher values (see H-R in Fig. 4*b*) [26,44-47], including those above 5 wt.%, correspond to higher pressures (approximately 10 MPa), while at lower (including ambient) pressures, gravimetric densities are below 1 wt.% (see A-G in Fig. 4*b*) [26,27,34,40,43], except for the results of our study (see D and E in Fig. 4*b*). Although the gravimetric densities obtained from our simulations are similar to those reported by various experiments and Monte Carlo (MC) simulations (cf. D with J [46], O [47], P [47], and S [39] as well as E with M [46] and Q [77] in Fig. 4*b* and Table S1), the results convincingly show how to increase the hydrogen storage capacity of SWNTs under ambient conditions.

Conclusions

In this study, we investigated the effect of endohedral Ni atoms on hydrogen physisorption on the SWNT surface by means of reactive MD simulations. The results show that Ni atoms weakly interact with the interior of SWNT due to the confinement effect. Consequently, this effect, along with the addition of Ni, collectively contributes to an increase in the gravimetric density of physisorbed hydrogen on SWNT upon increasing the volume fraction of endohedral Ni atoms. In particular, for SWNTs with endohedral Ni atoms at volume fractions of 0, 4, 22, and 56%, the gravimetric density

of physisorbed H_2 molecules was found to be 1.86, 2.32, 2.75, and 2.92 wt.%, respectively. Although these values are qualitatively close to the experimental and theoretical data, the results were obtained for nearly ambient pressure, which is approximately two orders of magnitude lower than the hydrogen pressures used for conventional hydrogen storage. In general, this study contributes to the atomic-level understanding of the role of endohedral transition metal nanocatalysts in enhancing the hydrogen storage capacity of carbon nanotubes under ambient conditions.

Acknowledgments

This research was carried out within the framework of the F-FA-2021-512 project, granted by the Agency for Innovative Development of the Republic of Uzbekistan. Additionally, P.N. and E.C.N. gratefully acknowledge the support by the Fund of Scientific Research Flanders (FWO), Belgium, Grant number 1261721N. The simulations were conducted using the computational resources available at the Institute of Ion-Plasma and Laser Technologies, Academy of Sciences of Uzbekistan. In addition, the computational resources and services used in this work were partially provided by the HPC core facility CalcUA of the Universiteit Antwerpen and VSC (Flemish Supercomputer Center), funded by the FWO and the Flemish Government.

References

[1] T. Kober et al., *Global energy perspectives to 2060–WEC's World Energy Scenarios 2019*, Energy Strategy Reviews **31**, 100523 (2020).

[2] Q. Hassan et al., *Renewable energy-to-green hydrogen: A review of main resources routes, processes and evaluation*, Int. J. Hydrogen Energy **48**, 17383 (2023)

[3] Y.-P. Chen, *Nanostructured Materials for Next-Generation Energy Storage and Conversion: Hydrogen Production, Storage, and Utilization* (Springer Berlin Heidelberg, New York, NY, 2017).

[4] R. Krishna et al., *Hydrogen Storage for Energy Application*. In Hydrogen storage. IntechOpen (2012). http://dx.doi.org/10.5772/51238

[5] H. Barthélémy et al., *Hydrogen storage: Recent improvements and industrial perspectives*. International Journal of Hydrogen Energy, 42, 7254 (2017).

[6] N. L. Rosi et al., *Hydrogen Storage in Microporous Metal-Organic Frameworks*, Science **300**, 1127 (2003).

[7] A. C. Dillon et al., *Storage of Hydrogen in Single-Walled Carbon Nanotubes*, Nature **386**, 6623 (1997).

[8] A. Züttel et al., *Hydrogen Storage in Carbon Nanostructures*, International Journal of Hydrogen Energy **27**, 203 (2002).

[9] S.I. Orimo et al., *Complex hydrides for hydrogen storage*. Chemical Reviews, 107, 4111 (2007).

[10] B. Sakintuna et al., *Metal hydride materials for solid hydrogen storage: a review*. International journal of hydrogen energy **32**, 1121 (2007).

[11] M. Aziz, *Liquid hydrogen: A review on liquefaction, storage, transportation, and safety*. Energies **14**, 5917 (2021).

[12] M. R. Usman, *Hydrogen storage methods: Review and current status*. Renewable and Sustainable Energy Reviews **167**, 112743 (2022).

[13] T. Q. Hua et al., *Technical assessment of compressed hydrogen storage tank systems for automotive applications*. International Journal of Hydrogen Energy, **36**, 3037 (2011).

[14] W. Peschka, *Liquid hydrogen: fuel of the future*. Springer Science & Business Media (2012).

[15] R. E. Morris et al., *Gas Storage in Nanoporous Materials*, Angewandte Chemie International Edition **47**, 4966 (2008).

[16] M. G. Nijkamp et al., *Hydrogen Storage Using Physisorption – Materials Demands*, Appl. Phys. A **72**, 619 (2001).

[17] A. Schneemann et al., *Nanostructured metal hydrides for hydrogen storage*. Chemical Reviews 118, 10775 (2018).

[18] I. P. Jain et al., *Novel Hydrogen Storage Materials: A Review of Lightweight Complex Hydrides*, Journal of Alloys and Compounds **503**, 303 (2010).

[19] M. P. Suh et al., *Hydrogen storage in metal–organic frameworks*. Chemical Reviews **112**, 782 (2012).

[20] R. Ströbel et al., *Hydrogen storage by carbon materials*. Journal of power sources **159**, 781 (2006).

[21] L. Zhou, *Progress and problems in hydrogen storage methods*. Renewable and Sustainable Energy Reviews **9**, 395 (2005).

[22] J. L. C. Rowsell et al., *Strategies for Hydrogen Storage in Metal-Organic Frameworks*, Angewandte Chemie International Edition **44**, 4670 (2005).

[23] K. Xia et al., *An Unusual Method to Prepare a Highly Microporous Carbon for Hydrogen Storage Application*, Materials Letters **100**, 227 (2013).

[24] L. J. Murray et al., *Hydrogen storage in metal–organic frameworks*. Chemical Society Reviews **38**, 1294 (2009).

[25] Y. H. Hu & L. Zhang, *Hydrogen storage in metal–organic frameworks*. Advanced Materials **22**, E117 (2010).

[26] C. Liu et al., *Hydrogen Storage in Single-Walled Carbon Nanotubes at Room Temperature*, Science **286**, 1127 (1999).

[27] H. Takagi et al., *Adsorptive Hydrogen Storage in Carbon and Porous Materials*, Materials Science and Engineering: B **108**, 143 (2004).

[28] G. Gundiah et al., *Hydrogen Storage in Carbon Nanotubes and Related Materials*, J. Mater. Chem. **13**, 209 (2003).

[29] J. L. Mendoza-Cortes et al., *A Covalent Organic Framework That Exceeds the DOE 2015 Volumetric Target for H_2 Uptake at 298 K*, J. Phys. Chem. Lett. **3**, 2671 (2012).

[30] H. Lee et al., *Hydrogen Desorption Properties of Multiwall Carbon Nanotubes with Closed and Open Structures*, Appl. Phys. Lett. **80**, 577 (2002).

[31] X. Li et al., *Hydrogen Uptake by Graphitized Multi-Walled Carbon Nanotubes under Moderate Pressure and at Room Temperature*, Carbon **39**, 2077 (2001).

[32] H. G. Shiraz et al., *Investigation of Graphene-Based Systems for Hydrogen Storage*, Renewable and Sustainable Energy Reviews **74**, 104 (2017).

[33] S. Iijima, *Helical Microtubules of Graphitic Carbon*, Nature **354**, 6348 (1991).

[34] M. Becher et al., *Hydrogen Storage in Carbon Nanotubes*, Comptes Rendus Physique **4**, 1055 (2003).

[35] R. Rakhi et al., *Synthesis and Hydrogen Storage Properties of Carbon Nanotubes*, International Journal of Hydrogen Energy **33**, 381 (2008).

[36] J. Lyu et al., *An Overview of the Recent Progress in Modifications of Carbon Nanotubes for Hydrogen Adsorption*, Nanomaterials **10**, 255 (2020).

[37] J. Li et al., *Theoretical Evaluation of Hydrogen Storage Capacity in Pure Carbon Nanostructures*. The Journal of Chemical Physics **119**, 2376 (2003).

[38] J. Lawrence et al., *High Pressure Saturation of Hydrogen Stored by Single-Wall Carbon Nanotubes*, Appl. Phys. Lett. **84**, 918 (2004).

[39] C. Liu et al., *Hydrogen Storage in Carbon Nanotubes Revisited*, Carbon **48**, 452 (2010).

[40] G. E. Ioannatos et al., *H_2 Storage on Single- and Multi-Walled Carbon Nanotubes*, International Journal of Hydrogen Energy **35**, 622 (2010).

[41] E. Mosquera-Vargas et al., *Hydrogen Storage in Purified Multi-Walled Carbon Nanotubes: Gas Hydrogenation Cycles Effect on the Adsorption Kinetics and Their Performance*, Heliyon **7**, e08494 (2021).

[42] Y.-J. Han et al., *Influence of Nickel Nanoparticles on Hydrogen Storage Behaviors of MWCNTs*, Applied Surface Science **415**, 85 (2017).

[43] N. R. Raravikar et al., *Temperature Dependence of Radial Breathing Mode Raman Frequency of Single-Walled Carbon Nanotubes*, Phys. Rev. B **66**, 235424 (2002).

[44] M. Hirscher, *Handbook of hydrogen storage*. Topics in Applied Physics, 12 (2010) http://dx.doi.org/10.1002/9783527629800

[45] R. Saito et al., *Electronic Structure of Chiral Graphene Tubules*, Appl. Phys. Lett. **60**, 2204 (1992).

[46] J. S. Arellano et al., *Interaction of Molecular and Atomic Hydrogen with (5,5) and (6,6) Single-Wall Carbon Nanotubes*, J. Chem. Phys. **117**, 2281 (2002).

[47] C.-C. Yang et al., *Electrochemical Hydrogen Storage Behavior of Single-Walled Carbon Nanotubes (SWCNTs) Coated with Ni Nanoparticles*, International Journal of Hydrogen Energy **35**, 2336 (2010).

[48] J. M. De Sousa et al., *Hydrogenation Dynamics Process of Single-Wall Carbon Nanotube Twisted*, Chemical Physics Letters **739**, 136960 (2020).

[49] J. Lee et al., *Hydrogen Storage and Desorption Properties of Ni-Dispersed Carbon Nanotubes*, Applied Physics Letters **88**, 143126 (2006).

[50] J. Xiao et al., *Toward Fundamentals of Confined Catalysis in Carbon Nanotubes*, J. Am. Chem. Soc. **137**, 477 (2015).

[51] L. Yu et al., *In- and Out-Dependent Interactions of Iron with Carbon Nanotubes*, J. Phys. Chem. C **116**, 16461 (2012).

[52] H. Shiozawa et al., *Nickel Clusters Embedded in Carbon Nanotubes as High Performance Magnets*, Sci Rep **5**, 1 (2015).

[53] U. Khalilov et al., *Catalyzed Growth of Encapsulated Carbyne*, Carbon **153**, 1 (2019).

[54] U. Khalilov et al., *Mechanisms of Selective Nanocarbon Synthesis inside Carbon Nanotubes*, Carbon **171**, 72 (2021).

[55] L. Guan et al., *Super-Long Continuous Ni Nanowires Encapsulated in Carbon Nanotubes*, Chem. Commun. **17**, 1988 (2004)

[56] C. Jo et al., *Magnetism of Fe, Co, and Ni Nanowires Encapsulated in Carbon Nanotubes*, Journal of Magnetism and Magnetic Materials **320**, 3256 (2008).

[57] D. Ugarte et al., *Nanocapillarity and Chemistry in Carbon Nanotubes*, Science **274**, 1897 (1996).

[58] X. Pan, X. Bao, *The Effect of Confinement inside Carbon Nanotubes on Catalysis*. Acc. Chem. Res. **44**, 553 (2011).

[59] A.P. Thompson et al., *LAMMPS - a flexible simulation tool for particle-based materials modeling at the atomic, meso, and continuum scales*, Comp. Phys. Commun. **271**, 108171 (2022).

[60] J. E. Mueller et al., *Development and validation of ReaxFF reactive force field for hydrocarbon chemistry catalyzed by nickel*. The Journal of Physical Chemistry C **114**, 4939 (2010).

[61] G. Chen et al., *Chemically doped double-walled carbon nanotubes: cylindrical molecular capacitors*. Physical Review Letters **90**, 257403 (2003).

[62] A.V. Bondi, *Van der Waals volumes and radii*, The Journal of Physical Chemistry, **68**, 441 (1964).

[63] A. Peigney et al., *Specific Surface Area of Carbon Nanotubes and Bundles of Carbon Nanotubes*, Carbon **39**, 507 (2001).

[64] H. Berendsen et al., *Molecular-Dynamics with Coupling to An External Bath*, The Journal of Chemical Physics **81**, 3684 (1984).

[65] J. Sun et al., *Molecular Dynamics Simulations of Melting Iron Nanoparticles with/without Defects Using a Reaxff Reactive Force Field*, Sci Rep **10**, 1 (2020).

[66] D. Nguyen Trong et al., *Molecular Dynamics Simulation of Bulk Cu Material Pseudo-Crystallization under Various Factors*, Applied Sciences **12**, 1 (2022).

[67] G. Bussi et al., *Canonical Sampling Through Velocity Rescaling*, The Journal of Chemical Physics **126**, 014101 (2007).

[68] U. Khalilov et al., *Microscopic mechanisms of vertical graphene and carbon nanotube cap nucleation from hydrocarbon growth precursors*. Nanoscale **6**, 9206 (2014).

[69] U. Khalilov et al., *How the Alignment of Adsorbed Ortho H Pairs Determines the Onset of Selective Carbon Nanotube Etching*, Nanoscale **9**, 1653 (2017).

[70] R. C. Haddon, *Chemistry of the Fullerenes: The Manifestation of Strain in a Class of Continuous Aromatic Molecules*, Science **261**, 1545 (1993).

[71] N. D. Yilmazer et al., *Ni_{55} Nanocluster: A Density Functional Theory Study of the Binding Energy of Nickel and Ethylene Adsorption*, Turkish Journal of Chemistry **36**, 55 (2012).

[72] U. Khalilov et al., *Nanoscale mechanisms of CNT growth and etching in plasma environment*. Journal of Physics D: Applied Physics **50**, 184001 (2017).

[73] S. Niyogi et al., *Chemistry of Single-Walled Carbon Nanotubes*, Acc. Chem. Res. **35**, 1105 (2002).

[74] E. Joselevich, *Electronic Structure and Chemical Reactivity of Carbon Nanotubes: A Chemist's View*, ChemPhysChem, **5**, 619 (2004).

[75] C. M. Brown et al., *Quantum rotation of hydrogen in single-wall carbon nanotubes*. Chemical Physics Letters **329**, 311 (2000).

[76] N. Faginas-Lago et al., *Adsorption of Hydrogen Molecules on Carbon Nanotubes Using Quantum Chemistry and Molecular Dynamics*. J. Phys. Chem. A 120, 6451 (2016).

[77] P. A. Owusu et al., *A Review of Renewable Energy Sources, Sustainability Issues and Climate Change Mitigation*, Cogent Engineering **3**, 1167990 (2016).